25th ABCM International Congress of Mechanical Engineering
October 20-25, 2019, Uberlândia, MG, Brazil

COB-2019-2128
VIBRATION ATTENUATION IN A FLEXIBLE ROTOR USING A SHAPE MEMORY ALLOY

Bŕbara Nara Teixeira Cunha
Orlando Tomaz da Silva Neto
LMEst - Structural Mechanics Laboratory, Federal University of Uberlândia, School of Mechanical Engineering, Av. João Naves de Ávila, 2121, Uberlândia, MG, 38408-196, Brazil
barbara.teixeira@ufu.br
orlandoparahy@ufu.br

Marco Túlio Santana Alves
Federal University of Bahia, Polytechnic School, Department of Mechanical Engineering, Rua Aristides Novis, 2, Federação, Salvador, BA, 40210-630, Brazil.
marco.alves@ufba.br

Aldemir Aparecido Cavalini Jr
Valder Steffen Jr
LMEst - Structural Mechanics Laboratory, Federal University of Uberlândia, School of Mechanical Engineering, Av. João Naves de Ávila, 2121, Uberlândia, MG, 38408-196, Brazil
aacjunior@ufu.br
vsteffen@ufu.br

Abstract. *The purpose of this paper is to present the numerical modeling of a flexible rotating shaft supported by two bearings. In this case, one of the bearings supports is composed of wires of shape memory alloy (SMA) for passive and semi-active vibration control purposes. The SMA wires are attached along the horizontal direction of the shaft, and its superelasticity behavior is used to perform the vibration control. The considered rotating machine is modeled using the finite element method, while the SMA is mathematically represented using the Brinson constitutive model. The numerical results demonstrate the effectiveness of the considered control approach.*

Keywords: *shape memory alloy, finite element, vibration control, rotordynamics*

1. INTRODUCTION

Rotary machines have been developing and improving over the years due to demand for production. However, they are not free from defects and cross critical speeds leading the system to undesirable amplitudes, consequently reducing the working life of the equipment (Mahfoud *et al.*, 2009). Besides, either abrupt stops and unplanned interruptions of the equipment are leading to economic losses, including risks to human lives (Smalley *et al.*, 1997). Therefore, the need for applying the vibration control techniques on rotors.

The control techniques performed to rotary machines are the form active, passive, and semi-active. In the active based form, it is possible to act in near real-time on system responses to reduce vibration amplitudes. However, this form requires a sophisticated electronic architecture, an external power source, and a high implementation cost. In contrast, devices known as absorbers or isolators work in the passive form and not expended energy on the system, and also operate in a restricted frequency range, thus having low control efficiency according to Fuller *et al.* (1990)

In semi-active approaches, vibration is attenuated by indirectly altering the physical parameters of the system rotating machine, such as damping and stiffness of the bearings with an external energy source, according to Cavalini *et al.* (2011). This method is advantageous as it allows for real-time vibration attenuation with reduced power consumption. These techniques can be applied to rotor systems by using the so-called smart materials that can adapt to the different working conditions of a system. Among the various types of materials, it is possible to mention piezoelectric materials, magnetorheological and electromagnetic fluids, electroactive polymers (hydrogels) and shape memory materials (Worden *et al.*, 2003).

According to Lagoudas (2008), SMA's have a higher working capacity per volume unit compared to other intelligent materials being also more effective at dissipating mechanical energy. They are considered excellent actuators to attenuate

vibration amplitudes. Besides, they can recover their shape when applied to a temperature field, even under high applied loads. Lagoudas (2008) shows that these alloys can recover from large deformations without presenting plastic deformations. This feature is associated with phase transformations (martensitic and austenitic) that occur in the presence of mechanical stress or with temperature variations, which are reversible (direct and reverse transformations).

According to Otsuka and Wayman (1998), the austenitic phase is characterized by high temperature and solid and cubic crystalline structure. In turn, the martensite presents the phase in low temperatures, a monoclinic structure with little symmetry and ductility. Due to the phase transformations, the SMA's present the memory effects of the shape and the superelasticity, (Emiliavaca, 2016), being the superelasticity explored in the present contribution.

Pinto *et al.* (2011) found that for a vibratory system with a resilient element made up of SMA's, the Brinson constitutive model has a broader range of applications as it can be applied at any temperature. Furthermore, it has shown in numerical tests that SMAs are capable of reducing the vibration amplitudes of mechanical systems through the superelastic effect. As such, they are widely used as dynamic vibration absorbers.

Nagaya *et al.* (1987) used SMA's springs coupled to a steel-spring rotor bearing for active control with antagonistic actuation in the critical speed passage. Liu *et al.* (1994) proposed fixed SMA wires to the hydrodynamic bearing to control vibration by dissipating energy and changing stiffness as a function of deformation. When the rotor accelerated there was a reduction in stiffness and while the rotor decelerated it increased the stiffness. The results showed that the vibration amplitudes and forces were significantly attenuated. Nie and Yan (2000) have designed an intelligent system for the critical speed of a rotary machine. For this, they used an active rigidity modification system, and the SMA wires were driven only as actuators to position the wedge at the appropriate time. The results showed that the designed system is applicable to control the vibrations of an aero-engine at the critical speeds.

He *et al.* (2006) have proposed an SMA-based self-optimized support system to attenuate vibration amplitudes so that the rotor safely passes critical speed. For this, an SMA spring vibration absorber was proposed for the rotary system bearing. They are capable of altering the rigidity of the bearing, thus efficiently controlling the vibration amplitudes. In a recent work Borges *et al.* (2016) analyzed the applicability of SMA's in an active bearing rotor and a Fuzzy logic-based temperature control system aiming to reduce rotor vibrations at the critical speeds. The results show reductions of up to 61.5% in peak amplitudes and 57.3% in signal RMS when passing through the resonance regions.

Thus, the principal objective of this paper is the numerical modeling in element finis of a flexible rotary machine that uses SMA in a suspended bearing because of the energy dissipation characteristics aiming for reductions in vibration amplitudes of the system.

2. METHODOLOGY

2.1 Rotor Model

The finite element model of the flexible rotor is represented by a matrix differential equation that describes the dynamic behavior of the system. This model is represented mathematically according to Eq. (1) (Lalanne and Ferraris, 1998).

$$[M]\{\ddot{x}(t)\} + [C + \dot{\phi}C_g]\{\dot{x}(t)\} + [K + \ddot{\phi}K_g]\{x(t)\} = \{F_{ext}(t)\} \tag{1}$$

where $[M]$ is the inertia matrix, $[C]$ is the damping, $[C_g]$ is the gyroscopic matrix, $[K]$ is the stiffness matrix, $[K_g]$ is a stiffness matrix resulting from the transient motion, $\{x(t)\}$ is the generalized displacement, $\{F_{ext}(t)\}$ is the external force vector, and $\dot{\phi}$ is the angular velocity of the rotor.

The damping considered was the proportional damping, shows by Eq. 2:

$$[C] = \alpha\,[M] + \beta\,[K] + C_{bearing} \tag{2}$$

where α and β are positive real constants.

The shaft was modeled by using Timoshenko's beam elements with two nodes and four degrees of freedom per node (two displacements and two rotations). Due to the size of the finite element matrices, the pseudo-modal method was used to solve the equations of motion. Thus, the physical coordinates x were changed to the modal coordinates q shown in Eq. (3).

$$x = \Phi q \tag{3}$$

where Φ is the modal matrix containing the m first vibration modes of the nongyroscopic, symmetric and undamped associated rotor.

Substituting Eq. (3) into Eq. (1) and multiplying the resulting expression by Φ^T, the reduced equation of motion of the rotor is obtained as follows:

$$[\tilde{M}]\{\ddot{q}\} + [[\tilde{C}] + \dot{\phi}[\tilde{C_g}]]\{\dot{q}\} + [[\tilde{K}] + \ddot{\phi}[\tilde{K_g}]]\{q\} = [\tilde{Q}] \tag{4}$$

where $[\tilde{M}] = \Phi^T[M]\Phi$; $[\tilde{C}] = \Phi^T[C]\Phi$; $[\tilde{C_g}] = \Phi^T[C_g]\Phi$; $[\tilde{K}] = \Phi^T[K]\Phi$; $[\tilde{K_g}] = \Phi^T[K_g]\Phi$; $[\tilde{Q}] = \Phi^T[Q]\Phi$.

The equation solution Eq. (4) results in a response vector described in modal coordinates. Applying Eq. (3), it is possible to convert the dynamic response in the modal domain to physical coordinates.

2.2 Constitutive model for shape-memory materials of Brinson

In the present paper, the Brinson model is used the represent the SMA (Brinson, 1993) and (Brinson and Huang, 1996). Brinson's constitutive model is a unidimensional model based on the Tanaka model Tanaka (1986). In this paper, due to the arrangement of the suspended bearing, only the case of traction was considered, although Brinson's constitutive model includes both traction and compression. The volume fraction of martensitic in the SMA is calculated by Eq. 5. Thus, the governing equation is presented in Eq. 6:

$$\xi_M = \xi_{TM} + \xi_{DM} \tag{5}$$

$$\sigma = E(\epsilon - \epsilon_R\,\xi_M) \tag{6}$$

where ξ_M is the volume fraction of martensitic in the SMA, ξ_{TM} is the volume fraction of twinned martensite, ξ_{DM} is the volume fraction of detwinned martensite, σ is the stress, E is the Young's modulus, ϵ is the deformation and ϵ_R is the residual deformation.

As only the superelastic effect will be exploited, it is guaranteed that the operating temperature will be above the final austenitization temperature A_f. Thus, the volume fraction of twinned martensite ξ_{TM} is zero. Hence, the total volume of martensite is $\xi_M = \xi_{DM}$. It is worth mentioning that the thermoelastic effect is neglected, as are the effects of volume change on transformation. Regarding Eq. (6)Young's modulus can be calculated as shows Eq. (7).

$$E(T,\sigma) = E_A + \xi(E_M - E_A) \tag{7}$$

$$\epsilon(T,\sigma) = \frac{\sigma}{E(T,\sigma)} + \epsilon_R[\xi(T,\sigma)] \tag{8}$$

where E_A is Young's modulus of austenite, E_M is Young's modulus of martensite and T is the temperature.

The tangential Young's modulus is given by $E_t = \frac{\partial\sigma}{\partial\epsilon}$. The partial derivatives for Young's modulus and deformations are presented in the equations below.

$$\frac{\partial\epsilon}{\partial\sigma} = \frac{1}{E^2}\left(E - \sigma\frac{\partial E}{\partial\sigma}\right) + \epsilon_R\frac{\partial\xi}{\partial\sigma} \tag{9}$$

$$\frac{\partial\epsilon}{\partial T} = \frac{1}{E^2}\left(E - \sigma\frac{\partial E}{\partial T}\right) + \epsilon_R\frac{\partial\xi}{\partial T} \tag{10}$$

$$\frac{\partial E}{\partial\sigma} = (E_M - E_A)\frac{\partial\xi}{\partial\sigma} \tag{11}$$

$$\frac{\partial E}{\partial T} = (E_M - E_A)\frac{\partial\xi}{\partial T} \tag{12}$$

Substituting Eq. (11) into Eq. (9) and Eq. (12) into Eq. (10):

$$\frac{\partial\epsilon}{\partial\sigma} = \frac{1}{E} - \frac{\sigma(E_M - E_A)}{E^2}\frac{\partial\xi}{\partial\sigma} + \epsilon_R\frac{\partial\xi}{\partial\sigma} \tag{13}$$

$$\frac{\partial\epsilon}{\partial T} = -\frac{\sigma(E_M - E_A)}{E^2}\frac{\partial\xi}{\partial T} + \epsilon_R\frac{\partial\xi}{\partial T} \tag{14}$$

The strain can be write as:

$$\sigma - \sigma_0 = E(\xi)\epsilon - E(\xi_0)\epsilon_0 \tag{15}$$

in which the sub-index 0 means initial conditions.

For the formulation of the model used in this paper, the boundary stresses of the forward and reverse transformation regions must be known and calculated by Eq. (16), Eq. (17), Eq. (18) and Eq. (19).

$$\sigma_{\hat{f}_s} = C_M \left(T - M_s\right) \tag{16}$$

$$\sigma_{\hat{f}_f} = C_M \left(T - M_f\right) \tag{17}$$

$$\sigma_{\hat{r}_s} = C_A \left(T - A_s\right) \tag{18}$$

$$\sigma_{\hat{r}_f} = C_A \left(T - A_f\right) \tag{19}$$

where $\sigma_{\hat{f}_s}$ is the initial strain of the direct transformation region, $\sigma_{\hat{f}_f}$ is the final strain of the direct transformation region, $\sigma_{\hat{r}_s}$ is the initial strain of the inverse transformation region, $\sigma_{\hat{r}_f}$ is the final strain of the inverse transformation region, M_s is the is the martensitic start temperature M_f is the is the martensitic finish temperature, A_s is the is the austenitic start temperature, A_f is the is the austenitic finish temperature. C_M is the is the stress influence coefficient of martensite,C_A is the stress influence coefficient of austenite and T is the working temperature of the SMA.

It is worth mentioning that the austenitic phase is stable when $T > A_f$, and the martensitic phase is stable when $T < M_f$. Equation (20) shows the martensitic evolution in terms of foward transformation ($k_{\hat{f}s}$).

$$k_{\hat{f}s} = \frac{\sigma - \sigma_{\hat{f}s}}{\sigma_{\hat{f}f} - \sigma_{\hat{f}s}} \tag{20}$$

The defined hardening function used in this paper was defined by Enemark *et al.* (2015), $f_{\hat{f}} = f\left(k_{\hat{f}}\right)$.

$$\xi_M = \xi_0 + \left(1 - \xi_0\right) f_{\hat{f}} \tag{21}$$

$$\frac{\partial \xi_M}{\partial T} = \frac{\left(1 - \xi_0\right) f'_{\hat{f}}}{M_f - M_s} \tag{22}$$

$$\frac{\partial \xi_M}{\partial \sigma} = \frac{\left(1 - \xi_0\right) f'_{\hat{f}}}{\sigma_{\hat{f}_f} - \sigma_{\hat{r}_f}} \tag{23}$$

where $f'_{\hat{f}} = \frac{\partial \xi_M}{\partial T}$

Similarly to the case of inverse transformation, the same parameters of Eq. (20), Eq. (21), Eq. (22) and Eq. (23). are calculated for the reverse transformation, except that as a function of the index $\hat{r}$.

Through the isocurves of the martensite fraction of the Brinson model, it was stipulated to a feasible deformation and initial temperature, aiming to potentiate the transformation of phases forward and reverse. For this paper the initial parameters chosen to be implemented in the iterative program were $\xi_0 = 50\%$, $T_0 = 30°C$, and $\epsilon_0 = 3\%$. Subsequently, from the initial deformation, the angle $\alpha_0 = 12$ was also determined, resulting in a maximum displacement of the bearing of $b = 17.1mm$.

In the present contribution, wires of SMA are constituted of nickel and titanium alloy (Ni-Ti) and have a thermomechanical behavior capable of causing changes between austenite and martensite.

Bekker and Brinson (1998) proposed a cosine function representing the hardening function for forward and reverse transformations. In this paper, is employed a cubic Bézier curve proposed by (Enemark *et al.*, 2015) and Alves *et al.* (2015), wich the parametres are n_1, n_2, n_3, and n_4. Table 1 presents its geometric and thermomechanical properties. It is worth mentioning that the thermomechanical properties of the SMA wires were obtained according to (Alves *et al.*, 2015).

Table 1: Properties SMA [adapted from (Alves *et al.*, 2015)].

SMA Wire Diameter (mm)	0.25
SMA Wire Length (mm)	40
E_A (GPa)	32.47
E_M (GPa)	18
A_s (°C)	-12.78
A_f (°C)	8.42
M_s (°C)	-3.47
M_f (°C)	13.47
n_1	0.737
n_2	0.999
n_3	0.580
n_4	0.998

2.3 Rotor model with SMA represented by finite element method

Figure 1 shows the general outline of the rotor test rig used in the numerical applications performed in the present work. It is composed of a flexible steel shaft with 600 mm length and 8 mm diameter ($E = 205GPa$, $\rho = 7850\frac{Kg}{m^3}$, and $\nu = 0.29$), two rigid steel discs with 100 mm diameter and 0.753 kg ($\rho = 7850\frac{Kg}{m^3}$), and two self-alignment ball bearings.

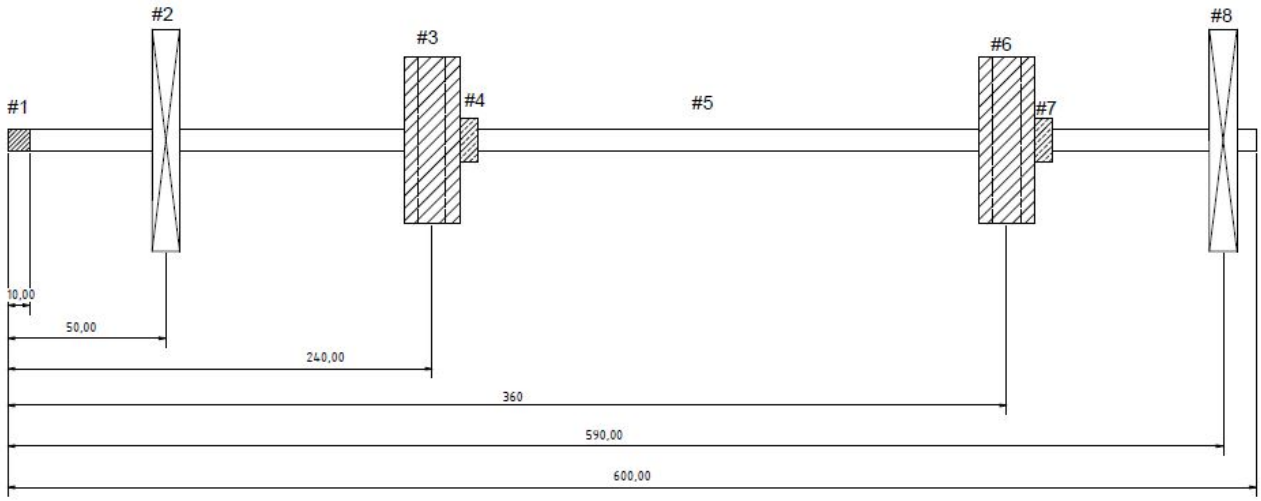

Figure 1: Rotor scheme

In Fig. 1 #1 presents the coupling between the motor and shaft, #2 is the support of ones of the bearing, #5 is the flexible shaft, #3 and #6 are the discs of the rotation machine, #4 and #7 are the brass bushings and #8 is the suspended bearing by wires of shape memory alloys in the horizontal direction. It is worth mentioning that the SMA wires are anchored and pre-tensioned only in the horizontal direction. Besides, they are positioned so that they work antagonized from each other and always pulled. Figure 3 presented the details to the bearing with the wires of SMA.

Figure 2 shows the schematic drawing of the steel disc with the brass bushings. The and through the Inventor ® design software that calculated as inertia properties of the mass of the set (disc + bushing). Table 1 shows the property's geometrics of the shafts and the disc.

Table 2: Properties disc.

Set (disc + bushing) mass (g)	808.71
Set (disc + bushing) density (g/cm^3)	8.66
Mass Unbalance $(g.mm)$	100
Idx $(g.mm^2)$	608124.09
Idz $(g.mm^2)$	1185335.38

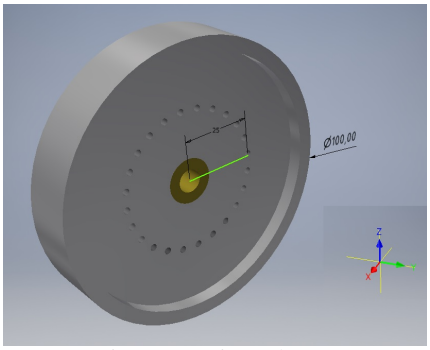

Figure 2: Disc scheme

The mathematical model of the suspended bearing constituted by the SMS was the same considered by (Alves *et al.*, 2015) shown in Fig. 3 and Fig.4. With the initial to the initial parameters of deformation, temperature, and displacement defined in section 2.1, it is calculated the resulting force in the suspend bearing by equation 24.

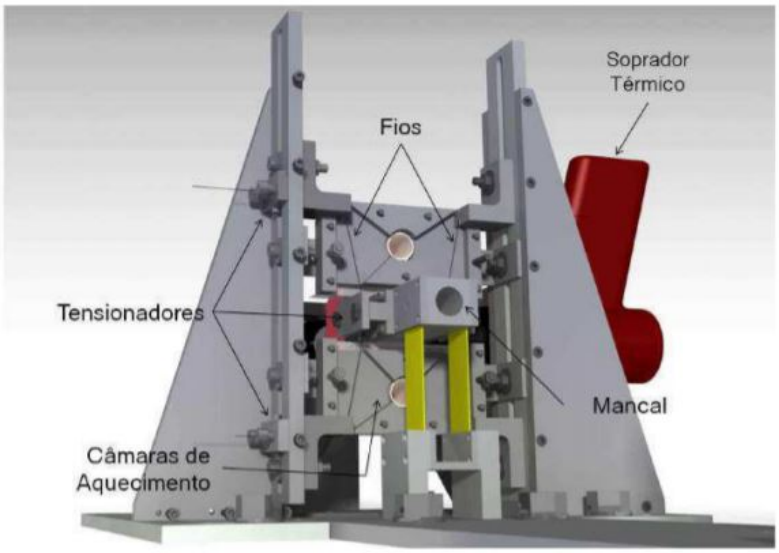

Figure 3: Suspended bearing scheme [adptaded from (Alves *et al.*, 2015)]

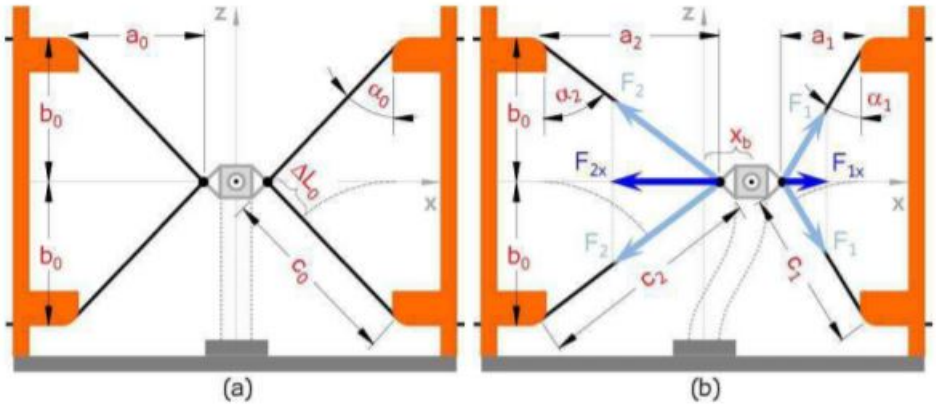

Figure 4: Bearing scheme Suspended by wire of SMA's (a) rotor at rest (pre-tensioned) and (b) rotor in operation. [adptaded from (Alves *et al.*, 2015)]

According to (Alves *et al.*, 2015) the force on the SMA wires is given by Eq.(24) .

$$F_{SMA} = F_{1x} - F_{2x} \tag{24}$$

Where F_{1x} and F_{2x} represent the forces that the SMA's wires exercises on the bearing in the direction horizontal and are given by Eq.(25) and Eq.(26).

$$F_{1x} = \frac{2\sigma_2 A\left(x_p - x_b\right)}{\sqrt{x_b^2 - 2x_b L\left(1+\epsilon_0\right)\sin\alpha_0 + \left[\left(1+\epsilon_0\right)L\right]^2}} \tag{25}$$

$$F_{2x} = \frac{2\sigma_2 A\left(x_p - x_b\right)}{\sqrt{x_b^2 + 2x_b L\left(1+\epsilon_0\right)\sin\alpha_0 + \left[\left(1+\epsilon_0\right)L\right]^2}} \tag{26}$$

where σ_2 is the axial tension on the wire, A is the cross-sectional area of the wire x_p relative displacement due to static pretension generation, x_b is the bearing offset L is the relaxed length of wire, ϵ_0 is the initial deformation, α_0 is the angle between the wire and the vertical for the rotor at rest (pre-tensioned). Table 2 shows the properties of the stiffness and damping of the bearings in this model. Also, the stiffness rotational of the couple considered in this work is 100 N/m.

Table 3: Dynamic properties of bearings

	Mass (Kg)	Stiffness x (N/m)	Stiffness z (N/m)	Damping (Ns/m) x	Damping z (Ns/m)
Bearing 1	0.014	$1.4 \cdot 10^5$	$2.4 \cdot 10^5$	0.5	0.05
Bearing 2	0.540	$8.0 \cdot 10^4$	$8.0 \cdot 10^4$	0.5	0.05

3. RESULTS

This section presents an analysis of results obtained from numerical approaches. The main objective of this paper is the use of SMA in the rotor with temperature variation for vibration reduction. The finite element model of the rotor is represented by 60 elements that were implemented in Matlab ® of this present contribution.

Numerical simulations have been carried along the run-up operation to predict the rotor vibration responses with the SMA wires installed in the bearing 2 (see Fig. 3 and Fig.4). Figure 5 illustrates the displacements in the steady-state along the x and z directions, with the SMA-bearing off and on with comparisons the temperature.

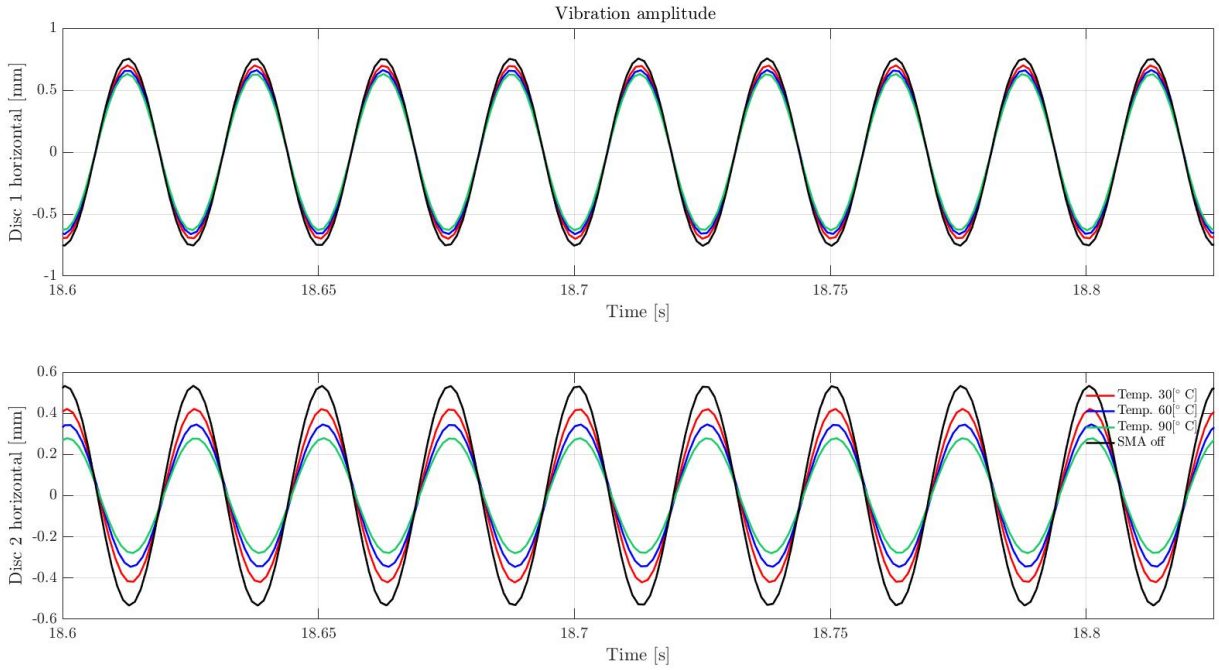

Figure 5: Vibration responses of the rotor (Steady-State).

Note that a considerable displacement reduction resulted (around 41% reduction) without the wires of SMA and the with wires ate temperature at 90 $°C$. In this case, a pseudoelastic condition and 3% strain (pre-tension) have been assumed for the SMA wires as the initial value.

Figure 6 shows the force applied by the SMA in the rotor were obtained considering a linear run-up condition from 0 to 4800 RPM in 100 seconds which compares the forces in to 3 differentes temperatures (a 30 $^{\circ}C$, a 60 $^{\circ}C$ e 90 $^{\circ}C$)

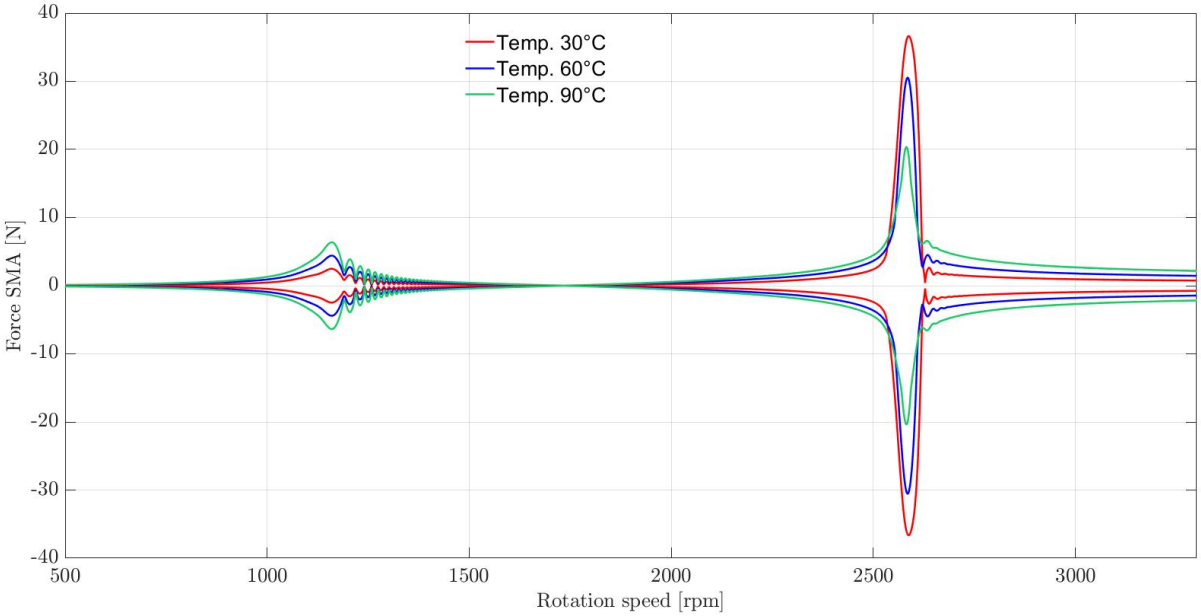

Figure 6: Force acting on the SMA wires.

Figure 7 presents the behavior of the vibration amplitudes of the bearing and disc 2, both in the horizontal direction. The rotor is subjected to heating ambient temperature considered to be 25 $^{\circ}C$ to 90 $^{\circ}C$.

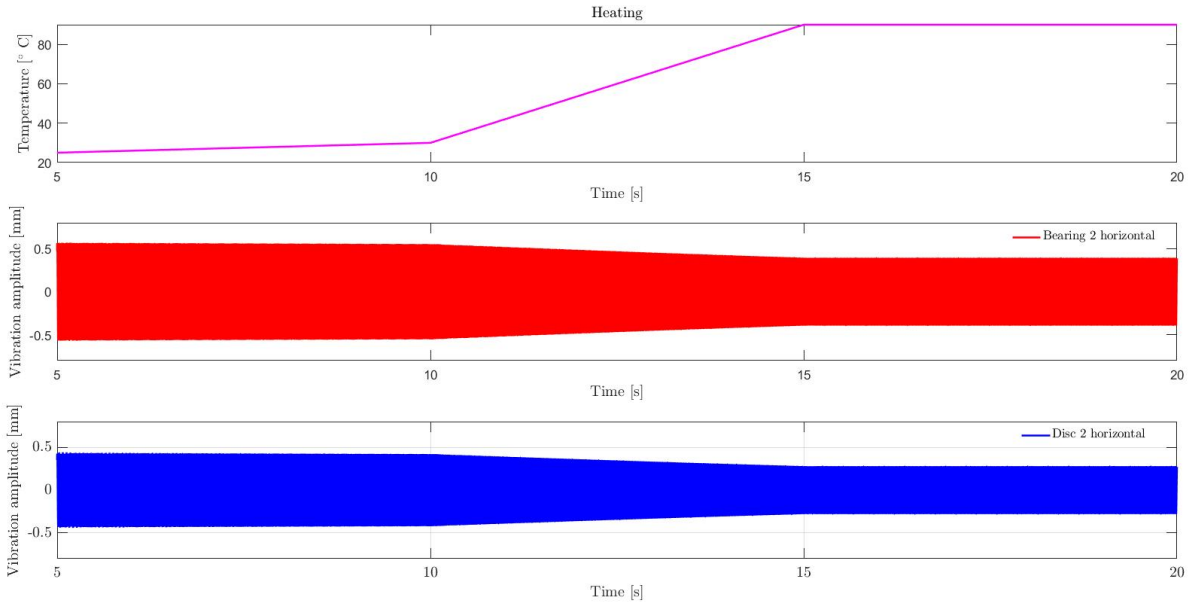

Figure 7: Vibration responses of the Bearing 2(direction horizontal) (Run-up).

Therefore, it was noted that the displacements were reduced until to stabilize when the temperature remained constant at 90 ^{circ}C. It is worth mentioning that the time from 0 to 5, the temperature considered is to temperature ambient. Moreover, this interval was not computed in Fig. 7 because it represents the steady-state stabilization time of the numerical and physical model.

4. DISCUSSIONS AND CONCLUSSIONS

In this paper, the efficiency of SMA wires for vibration attenuation purposes in flexible rotating machines was evaluated. For this aim, a horizontal rotor composed of a flexible shaft, two rigid discs, and two bearings was used. In this case, SMA wires were installed in one of the bearings.

The results show that the vibration amplitude decreases as the SMA temperature increases. The wire's force of SMA wires increases according to the temperature for the critical velocity first and has an inverse behavior for the third critical velocity.

The temperature variations modify the critical rotor speed allowing vibration amplitude reduction. This characteristic can be used as a smart mechanism for crossing critical speeds.

The steady-state tests operating at the first critical speed reveal that the suspended SMA wires constitute an efficient passive vibration control element. In this simulation, there was a reduction of around 41 % of vibration levels with the use of the SMA alloy in the temperature of 90 $^{\circ}C$. Therefore, the obtained results demonstrated the effectiveness of the considered approach.

The housing of bearing 2 behaves like a single degree of freedom damped dynamic system whose characteristics of stiffness and damping depend on the SMA wires thermomechanical properties.

It is possible to conclude that this system vibrates around a point of static equilibrium, which is defined by static deformation (pre-tensile load). Theoretically, this is a statically balanced system. Dynamic loads are given by the residual force unbalance and SMA wires force;

Also, the pre-tensile load is an important design parameter for SMA suspension wires in rotor dynamics. The configuration of the wires should be close to the initial martensite transformation stress to allow for deformation due to loading variation and also to recover deformation by temperature effect. Moreover, the passive control using SMA wires is a simple way of controlling the dynamic response of rotors since it takes advantage of an intrinsic characteristic of SMA.

5. ACKNOWLEDGEMENTS

The authors are thankful for the financial support provided to the present research effort by CNPq (574001/2008-5,304546/2018-8, and 431337/2018-7), FAPEMIG (TEC-APQ-3076-09, TEC-APQ-02284-15, TEC-APQ-00464-16, and PPM-00187-18), and CAPES through the INCT-EIE.

6. REFERENCES

Alves, M.T.S. *et al.*, 2015. "Controle de vibrações em máquinas rotativas usando ligas com memória de forma".

Bekker, A. and Brinson, L.C., 1998. "Phase diagram based description of the hysteresis behavior of shape memory alloys". *Acta materialia*, Vol. 46, No. 10, pp. 3649–3665.

Borges, J.M. *et al.*, 2016. "Controle de um sistema dinâmico rotativo utilizando mancais com atuadores lmf".

Brinson, L.C., 1993. "One-dimensional constitutive behavior of shape memory alloys: thermomechanical derivation with non-constant material functions and redefined martensite internal variable". *Journal of intelligent material systems and structures*, Vol. 4, No. 2, pp. 229–242.

Brinson, L. and Huang, M., 1996. "Simplifications and comparisons of shape memory alloy constitutive models". *Journal of intelligent material systems and structures*, Vol. 7, No. 1, pp. 108–114.

Cavalini, A.A., Galavotti, T.V., Morais, T.S., Koroishi, E.H. and Steffen, V., 2011. "Vibration attenuation in rotating machines using smart spring mechanism". *Mathematical Problems in Engineering*, Vol. 2011.

Emiliavaca, A., 2016. *SMArt MORPHING WING um protótipo de asa adaptativa acionada por micromolas de liga com memória de formal*. Master's thesis, Universidade Federal de Campina Grande, Campina Grande.

Enemark, S., Santos, I. and Savi, M.A., 2015. "Shape memory alloys applied to improve rotor-bearing system dynamics-an experimental investigation". In *XVII International Symposium on Dynamic Problems of Mechanics*.

Fuller, C., Gibbs, G. and Silcox, R., 1990. "Simultaneous active control of flexural and extensional waves in beams". *Journal of Intelligent Material Systems and Structures*, Vol. 1, No. 2, pp. 235–247.

He, Y.Y., Oi, S., Chu, F.L. and Li, H.X., 2006. "Vibration control of a rotor–bearing system using shape memory alloy: Ii. experimental study". *Smart Materials and Structures*, Vol. 16, No. 1, p. 122.

Lagoudas, D.C., 2008. *Shape Memory Alloys, Modeling and Engineering Applications*. Springer Science Business Media.

Lalanne, M. and Ferraris, G., 1998. *Rotordynamics prediction in engineering*, Vol. 2. Wiley.

Liu, B., Yan, L., Li, Q. and Zhu, Z., 1994. "Vibration control of a rotor system utilizing a bearing housing with controllable spring nonlinearity". In *ASME 1994 International Gas Turbine and Aeroengine Congress and Exposition*. Citeseer, pp. V005T14A007–V005T14A007.

Mahfoud, J., Hagopian, J.D., Lévecque, N. and Steffen Jr, V., 2009. "Experimental model to control and monitor rotating machines". *Mechanism and Machine Theory*, Vol. 44, No. 4, pp. 761–771.

Nagaya, K., Takeda, S., Tsukui, Y. and Kumaido, T., 1987. "Active control method for passing through critical speeds of

rotating shafts by changing stiffnesses of the supports with use of memory metals". *Journal of Sound and Vibration*, Vol. 113, No. 2, pp. 307–315.

Nie, J. and Yan, X., 2000. "Intelligent bearing system for passing through critical speed of aeroengine rotor by changing stiffness using sma wires". In *Materials science forum*. Vol. 327, pp. 99–102.

Otsuka, K. and Wayman, C., 1998. "Mechanism of shape memory effect and superelasticity". *Shape memory materials*, pp. 27–48.

Pinto, A.A. *et al.*, 2011. "Estudo teórico e numérico de modelos constitutivos de ligas com memória de forma e associação com sistemas vibratórios".

Smalley, A.J., Mauney, D.A. *et al.*, 1997. "Risk based maintenance of turbomachinery." In *Proceedings of the 26th Turbomachinery Symposium*. Texas A&M University. Turbomachinery Laboratories.

Tanaka, K., 1986. "A thermomechanical sketch of shape memory effect: one-dimensional tensile behavior". *Res. Mechanica*, Vol. 18, pp. 251–263.

Worden, K., Bullough, W.A. and Haywood, J., 2003. *Smart technologies*. World Scientific.

7. RESPONSIBILITY NOTICE

B.N.T. Cunha, O.T. Silva Neto, M.T.S. Alves, A.A. Cavalini Jr, and V. Steffen Jr are the only responsible for the printed material included in this paper.